Transportation Research Part E 206 (2026) 104597

Contents lists available at ScienceDirect

Transportation Research Part E

journal homepage: www.elsevier.com/locate/tre

Trade dynamics of the global dry bulk shipping network

Yan Li [a,*], Carol Alexander [a], Michael Coulon [a], István Zoltán Kiss [b,c]

[a] Business School, University of Sussex, BN1 9RH, Falmer Brighton, United Kingdom
[b] Network Science Institute, Northeastern University London, Devon House 58 St Katharine's Way, E1W 1LP, London, United Kingdom
[c] Department of Mathematics, Northeastern University, 02115, MA, Boston, USA

ARTICLE INFO

Keywords:
Complex network
Transportation
Dry bulk shipping
Shipping network
Trade flow

ABSTRACT

The primary objective of this study is to determine how global shocks and commodity-specific geographical factors interact to shape the structure, resilience, and vulnerability of the dry bulk shipping network. To do so, we examine the global dry bulk shipping network and its coal, grain, and iron ore sub-networks from 2015 to 2023 using micro-level trade flow data. We find that these networks are highly concentrated around a small number of key export ports, with heavy-tailed degree distributions and strong core-periphery structures. However, the impact of external shocks is sharply commodity-specific: the COVID-19 pandemic triggered a major reorganisation of coal trade communities, while the war in Ukraine fragmented the grain network and drastically reduced Ukraine's exports. In contrast, iron ore trade patterns remained relatively stable during the same period. Small-world features are present mainly within the densely interconnected core of each commodity network, where bi-directional trades are observed, while most peripheral ports function as either importers or exporters only. These findings clarify how the interplay of geography, trade imbalance, and global disruptions shapes network structure and resilience, offering insights for supply chain risk management in maritime logistics.

1. Introduction

Dry bulk shipping, a segment of tramp shipping where vessels operate without fixed schedules or routes, accounts for approximately 80 % of global seaborne trade in volume (UNCTAD, 2019). It serves as the backbone of the world economy through the transport of essential raw materials. Despite its scale and significance, the structure and disruption dynamics of dry bulk shipping networks remain understudied, especially in comparison to container (liner) shipping. This gap limits the ability of policymakers, industry, port authorities, and commodity traders to anticipate, understand, and manage network risks and disruptions.

Unlike liner shipping which operates on regular published schedules, dry bulk shipping is shaped by irregular demand-driven movements, a diverse array of cargoes, and market segmentation. The characteristics of liner shipping, along with its network's centralised logistic system, and scale-free properties, have made it more appealing to researchers. In comparison, the inherent variability in trade flows make dry bulk networks more complex to analyse using conventional network science approaches (Ducruet, 2013, 2020).

Thus, most existing research has focused on container networks which benefit from standardised schedules and richer data. By contrast, dry bulk networks are complex, segmented, and governed by demand for specific commodities, as their routes are irregular, highly sensitive to geopolitical and market shocks, and evolve with global supply/demand cycles. Consequently, although dry bulk shipping plays a critical role in international trade and seaborne transportation, it has received far less academic attention than the liner shipping sector.

* Corresponding author.
E-mail address: yl702@sussex.ac.uk (Y. Li).

https://doi.org/10.1016/j.tre.2025.104597
Received 2 February 2025; Received in revised form 13 October 2025; Accepted 4 December 2025
Available online 12 December 2025

We address these gaps by analysing global dry bulk shipping as a series of trade flow networks observed over time, using micro-level data from 2015 to 2023. In addition to the full dry bulk network, we also focus on its coal, grain, and iron ore sub-networks that together account for over 60 % of dry-bulk volume, and examine how network structure changes during periods of major global disruption. The chosen period combines the most complete dataset available with coverage of unprecedented geopolitical and market shocks.

The main objective of this study is to reveal how major external shocks reshape the structure and resilience of the global dry bulk shipping network and its key commodity sub-networks. The static analysis characterises the organisation of each commodity network, highlighting both the similarities and contrasts among coal, grain, and iron-ore networks and the broader aggregate system. This baseline explains why shocks produce distinct structural responses across commodity networks. The temporal analysis then pinpoints when major structural breaks occurred and how community configurations were reorganised during shocks such as COVID-19 and the war in Ukraine.

To our knowledge, this is the first study to examine global dry-bulk shipping networks from a trade flow perspective. Most previous studies rely on ship movement or port-call data, which lack commodity-specific detail. Our approach directly analyses trade flow networks using micro-level cargo data, capturing the underlying patterns of commodity movement and demand that shape the evolution of the dry bulk system. This granularity enables data-driven analysis of how network properties respond to disruption and how vulnerability differs across commodities. These insights have direct value for stakeholders seeking to manage operational risk and strengthen the resilience of maritime logistics.

The remainder of the paper is organised as follows: Section 2 reviews the relevant literature; Section 3 describes the dataset and its limitations; Section 4 outlines the network methods; Section 5 presents the empirical results; and Section 6 concludes.

2. Literature review

Recent advances in tracking and mapping technologies, particularly those outlined in studies on big data in maritime networks (Ducruet, 2017a), have transformed the analysis of ship trajectories and the spatial structure of maritime transport networks. Much of the existing literature has concentrated on liner shipping networks (Ducruet et al., 2010a,b; Ducruet and Notteboom, 2012; Ducruet et al., 2020; Laxe et al., 2012; Tsiotas and Polyzos, 2015; Wang et al., 2016; Calatayud et al., 2017a,b; Liu et al., 2018; Pan et al., 2019; Cheung et al., 2020; Bai et al., 2023; Kanrak et al., 2019; Wei et al., 2025; Williams and Del Genio, 2014), which use network methods to provide valuable insights into hierarchical structure, with implications for network's connectivity, vulnerability and efficiency as well as trade patterns.

In contrast, tramp shipping, including oil tankers and dry bulk carriers, operates with much greater variability and unpredictability, akin to a taxi service in its responsiveness to real-time demand (Kaluza et al., 2010; Brancaccio et al., 2020). Far fewer studies focus specifically on dry bulk networks (notable exceptions include Kaluza et al., 2010; Ducruet, 2013; Cremaschini et al., 2024; Wei et al., 2025). Of these, Kaluza et al. (2010) identified how dry bulk carriers exhibit much greater randomness in their movement patterns than container ships and oil tankers. Furthermore, Ducruet (2013) highlights the importance of network diversity, port centrality, and the impact of the combination of various cargo types on network resilience and vulnerability. These studies use concepts such as multi-sector shipping networks to analyse relationships between flows of different cargo types, showing that ports handling more diversified commodities tend to be more central and resilient.

Recent work in tramp shipping by Cremaschini et al. (2024) and Wei et al. (2025) focus on the analysis of disruption and resilience in dry bulk contexts. Cremaschini et al. (2024) examine the structural disruption of Ukraine's maritime trade following the war in the region, showing how geopolitical conflict reshapes network connectivity, port hierarchy, and trade resilience. As an example of such patterns, they document a collapse in hub centrality and a growing reliance on external transshipment hubs, particularly in Turkey and Romania, which they term "hub dependence". While this offers valuable insight into the geopolitical contingencies of maritime logistics, the analysis is regional in scope and does not assess global impacts.

Partially addressing this gap, Wei et al. (2025) study the resilience of the global grain trade network during the COVID-19 pandemic, using AIS data combined with trade data, to compare networks from 2020 to 2021. Applying a multidimensional resilience framework, they distinguish four phases of network response, which consist of reliability, vulnerability, robustness, and recoverability. Subsequently they find that recovery trajectories vary by region. However, despite this emphasis on regional diversity, due to the scope of its data, the study does not account for the profound structural changes surrounding the subsequent the war in Ukraine. Given continued geopolitical instability, and that the war in Ukraine impacted particularly on grain trade, there remains a need for data-driven methods that identify and interpret commodity-specific structural shifts in real time.

While the above two studies compare networks before and after major shocks, most existing studies do not incorporate temporal analysis of global trade networks. Although recent advances in dynamic and multilayered network modelling have expanded possibilities in maritime research (Ducruet, 2017b), such approaches have not been widely applied. Our study addresses this gap by capturing both dynamic and commodity-specific variations in trade flows.

In addition to the lack of temporal analysis, existing studies typically rely on vessel movement or port call data, which record port call sequences but not origin-destination relationships for each commodity. This is a critical limitation: dry bulk shipping operates through distinct commodity sub-networks, each with unique geographical patterns and logistics. These networks are driven by demand for physical cargo (Stopford, 2008), not simply vessel movement, so commodity-specific flows cannot be precisely captured without actual trade flow data. Our study, along with Brancaccio et al. (2020), addresses this limitation by using micro-level commodity-specific trade flow data, enabling the analysis of laden voyages by commodity and clarifying how demand-driven flows shape network dynamics. By doing this, we can directly observe how external shocks reshape network structure and connectivity. Our approach

identifies the timing of structural breaks, as well as the differentiated impacts of shocks on coal, grain, and iron ore networks. These results provide insights for resilience planning and commercial decision-making, addressing both academic developments and industry needs.

Finally, the focus on micro-level shipping data distinguishes this study from other network-based research that relies mainly on macro-level trade data and often overlooks the specific dynamics revealed by actual ship movements (Iapadre and Tajoli, 2014; Klimek et al., 2015; Kiyota, 2022; Wei et al., 2022; Yin et al., 2024; Zhang et al., 2024). In contrast, our approach aligns with maritime economics, which emphasises "the physical quantity of cargo" over trade value and prioritises geographical regions rather than political states (Stopford, 2008). Instead of ranking export or import regions, we adopt a commodity-specific network perspective to analyse dry bulk shipping system from the demand side.

In summary, the literature reveals three main gaps: (1) a historical focus on container shipping over dry bulk trade flows; (2) insufficient attention to the demand-derived nature of the dry bulk shipping network structure; most studies do not capture the actual trade relationships that underpin the demand-driven seaborne transportation system; and (3) a lack of commodity-specific and temporal analysis of network changes under major external shocks. Our study addresses these gaps by using micro-level, commodity-disaggregated trade flow data to examine structural dynamics in global dry bulk shipping networks.

3. Data

For our analysis of dry bulk shipping networks, we use the Oceanbolt Maritime Market Intelligence dataset provided by Veson Nautical. This source offers comprehensive coverage of global dry bulk shipping activity from January 2015 to December 2023, drawing on AIS-derived records of vessel movements and trade flows.[1] The dataset contains detailed information on vessel identity, size, commodity types, timestamps, and the geographic coordinates for loading and discharging events, enabling robust analysis of both the spatial and temporal dimensions of trade flows. A sample of the full dataset is provided in Supplemental Materials A.

Prior to analysis, we performed critical data cleaning to ensure reliability. Voyages with unknown load or discharge ports were excluded, and non-trade-related flows such as "Transit" and "Yard" were removed. After these steps, the final dataset comprised over 16,000 ships and 1.67 million trade flows spanning 21 commodity categories.

Coal, grain, and iron ore (labelled major bulk) together account for 64 % of total seaborne dry bulk trade volume (measured in metric tonnes) over the study period, yet represent only 32 % of all trade flows. This difference reflects the operational realities of bulk shipping, where major bulks are shipped in larger quantities per voyage, while minor bulks account for a greater number of smaller, more fragmented flows.

A key limitation of the dataset is the relatively large share of voyages with unknown cargo types (see Table 7 in Supplementary Material A), which reflects the common challenge of incomplete cargo reporting in maritime data. While we acknowledge this limitation, the dataset remains sufficiently large and robust for structural analysis. Notably, coal, iron ore, and grain together account for 64 % of the total observed trade volume (34.7 out of 53.9 billion GT), confirming their dominance in the network despite the presence of unknown cargo flows.

The choice of this dataset enables commodity-specific network construction and temporal analysis at high resolution. This granularity allows us to examine differences in the structure and evolution of trade flows for each major dry bulk commodity, providing the foundation for the network analysis in subsequent sections. For each major commodity (grain, coal, and iron ore), we create separate sub-networks using the same port set. Using quarterly time windows (reflecting an average voyage of approximately 35 days) ensures well-connected snapshots for structural analysis and allows us to capture the evolution of network properties over time. Summary statistics for trade flow durations are provided in the Supplementary Material A.

Advantages of the trade flow dataset. Unlike standard port call data, trade flow data records only laden legs between load and discharge ports, thus directly representing existing trade relationships and excluding ballast legs. This approach avoids overestimating the trade flow network connectivity and allows direct integration with freight rate data, since each network edge corresponds to an economic transaction for a specific cargo type.

Additionally, trade flow data provides a more accurate representation of network centrality and clustering, particularly for voyages with multiple loads or discharges, as it captures actual cargo flows from the perspective of trade origin to destination. Further technical details and illustrative figures are provided in Supplementary Material A.

4. Methods

This section outlines the network analysis framework and statistical approaches to examine the structure and evolution of the global dry bulk trade flow shipping network and its key commodity sub-networks.

4.1. Network representation and construction

The dry bulk shipping network is constructed from micro-level trade flow data covering the period 2015–2023. In this framework, each node represents a seaport included in the dataset, and directed edges are established between ports whenever a trade flow is

[1] A trade flow here refers to a single laden leg between a load and discharge port, as distinct from a full vessel voyage, which may comprise multiple trade flows.

recorded from a load port to a discharge port. The resulting network is represented by an adjacency matrix, where the element A_{ij} is assigned a value of 1 if there is a trade flow from port i to port j, and 0 otherwise.

To account for the intensity of shipping activity, edge weights are incorporated based on the frequency of voyages, cargo volume, or deadweight tonnage associated with each connection. Both an aggregate network (encompassing all cargo types of trade flows in the data sample) and separate commodity-specific sub-networks (for coal, grain, and iron ore) are generated, allowing for analysis at commodity level.

For temporal analysis, the data are organised into a sequence of quarterly network snapshots. Each snapshot aggregates all trade flows occurring within a given quarter, providing a series of static networks through which structural changes and disruptions can be traced over time. As noted by Holme and Saramäki (2012) and Guinand and Pigné (2015), the snapshot method is widely used in empirical studies, including those in maritime and transport network analysis. Although such representations are static, the quarterly resolution provides sufficient granularity to capture key structural transitions in the dry bulk network over eight years, particularly in response to major events such as the COVID-19 pandemic and the war in Ukraine. Nevertheless, it should be acknowledged that the chosen window size may influence sensitivity to rapid, short-term changes, and future research could explore the utility of alternative temporal resolutions or event-based analyses as higher-frequency data become available.

4.2. Network properties and benchmarking

In general, networks are measured by various metrics. At the node level, degree centrality and strength centrality which incorporates edge weights, capture the connectivity and trade volume associated with each port. Analysis of degree distributions provides insight into network heterogeneity and the presence of ports with unusually high connectivity. In real-world networks, a power-law degree distribution is often associated with scale-free networks, where a small number of nodes are highly connected while the majority have few links (Barabási and Albert, 1999). However, as noted by Ducruet (2020), maritime transport networks are spatially embedded and constrained by geography; interpretation of degree distributions is therefore made with caution in light of these factors. Nevertheless, analysis of degree distribution remains relevant for understanding whether dry bulk trade is centralised, fragmented, or balanced across commodities.

At the global level, the average shortest path length (ASPL) measures the mean of the shortest paths between all pairs of ports and is used to assess network efficiency. The clustering coefficient, or transitivity, indicates the tendency for triadic closure among ports, capturing the likelihood that a port's neighbours are themselves interconnected. A short ASPL suggests that most ports can be reached with relatively few connections, while a high clustering coefficient implies significant local interconnectedness. Together, these metrics are used to evaluate the potential presence of a small-world property, where networks combine short path lengths with high clustering.

Here, the degree assortativity coefficient is computed to quantify whether ports with similar connectivity tend to trade with each other, with values ranging from –1 (disassortative) to +1 (assortative), akin to a correlation coefficient. This metric characterises the structural organisation of the network with respect to connectivity patterns.

To assess the statistical significance of observed structural features, we implement a null model by generating randomised networks that preserve the observed degree sequence. This configuration model serves as a baseline for comparison of metrics such as clustering coefficient and ASPL. We further adopt the benchmarking framework of Humphries and Gurney (2008) and Telesford et al. (2011), computing the σ and ω indices to quantify the degree of small-world-ness:

$$\sigma = \frac{C/C_{\text{rand}}}{L/L_{\text{rand}}} \tag{1}$$

$$\omega = \frac{L_{\text{rand}}}{L} - \frac{C}{C_{\text{latt}}} \tag{2}$$

where C is the observed clustering coefficient, L is the observed average path length, C_{rand} and L_{rand} are values from an equivalent random network, and C_{latt} denotes the clustering coefficient for a lattice network.

As argued by Telesford et al. (2011), it is insufficient to assess small-world structure by comparing C and L to their random equivalents alone, since σ is highly sensitive to small values of C_{rand}. Instead, it is important to identify where a network lies along the spectrum between lattices and random graphs. Lattices exhibit high clustering but long path lengths, whereas random graphs achieve very short path lengths but small clustering. Small-world networks combine both properties: they preserve the high clustering typical of lattices while also achieving the short average path lengths found in random networks, meaning that ports form tight trading groups but are still easily reachable across the wider network.

In practice, $\sigma > 1$ and $\omega \approx 0$ indicate small-world organisation ($C \gg C_{\text{rand}}$, $L \approx L_{\text{rand}}$). Values of $\omega > 0$ suggest random-like structure, while $\omega < 0$ indicates lattice-like organisation. This benchmarking ensures that clustering and path length are interpreted relative to appropriate null expectations, rather than in isolation.

4.3. Community structure analysis

Community structure is a key topological property of complex networks, describing the organisation of nodes into groups with dense internal connections and sparser links between groups (Pan et al., 2019). In trade flow networks, community structure analysis reveals historical and persistent relationships between countries or regions (Yin et al., 2024). This is particularly relevant in maritime

shipping, where global seaborne trade is shaped by physical and geopolitical constraints (Stopford, 2008), and the configuration of trade communities may shift significantly in response to exogenous shocks.

In this study, community detection is used to identify groups of ports that are more densely interconnected than with the rest of the network. This approach uncovers how global dry bulk trade is segmented into commodity- or region-based blocs, and enables the tracking of their evolution over time. In particular, it provides insight into the resilience and vulnerability of supply chains at the community level, especially during disruptions such as the COVID-19 pandemic or the war in Ukraine.

Identifying and understanding large-scale patterns in network connectivity is challenging, particularly when the network is large and its structure is not easily visualised (Newman, 2010). To address this, we employ the Louvain algorithm for community detection (Blondel et al., 2008), which is widely used for large-scale, weighted networks due to its balance of computational efficiency, scalability, and interpretability. The Louvain method operates through a two-step modularity optimisation process: it first locally maximises modularity by iteratively grouping nodes into communities, and then aggregates these communities to form a new, smaller network, repeating the process until no further modularity gain is possible. The resulting partitioning not only provides community assignments but also a modularity score that quantifies the strength of internal versus external connectivity within communities.

We select the Louvain algorithm over alternatives such as Infomap or Label Propagation because it offers a robust trade-off between performance and interpretability for our application. Infomap excels in detecting overlapping or hierarchical structures but can be less stable with weighted, directed graphs. Label Propagation is highly efficient but sensitive to random initialisation and less reliable in identifying persistent communities in empirical data (Ghasemian et al., 2019). In contrast, the Louvain algorithm is well-suited for weighted, undirected or directed networks, and has demonstrated robustness in maritime and transport studies. It produces results that are both computationally tractable and easily interpretable for policy and industry audiences. Full details of the Louvain implementation are provided in Supplementary Material B.

Finally, by combining community detection with temporal analysis of quarterly snapshots of the sub-networks, we are able to track the formation, merging, or fragmentation of specific commodity trade relationships over time. This enables us to assess the dynamic resilience and adaptability of the global dry bulk shipping system.

4.4. Distance matrix

To quantify the dissimilarity between quarterly networks, we construct a distance matrix based on pairwise comparisons of the adjacency matrices for each quarter, following Sugishita and Masuda (2021). Let $\mathbf{D}$ denote the $(n \times n)$ distance matrix, where n is the total number of quarters analysed, and each element d_{ij} represents the distance between networks G_i and G_j for quarters i and j.

The distance between two directed, unweighted networks G_i and G_j is calculated as:

$$D(G_i, G_j) = 1 - \frac{M(G_i \cap G_j)}{\sqrt{M(G_i)M(G_j)}}, \tag{3}$$

where $M(G_i)$ and $M(G_j)$ are the total number of edges in G_i and G_j, and $M(G_i \cap G_j)$ is the number of edges common to both networks. The denominator, $\sqrt{M(G_i)M(G_j)}$, is the geometric mean of the edge counts, ensuring that the metric is bounded between 0 and 1. A distance of 0 indicates structurally identical networks; a distance of 1 indicates no shared edges. This geometric normalisation provides a scale-invariant measure of structural dissimilarity, allowing meaningful comparisons across networks of varying sizes.

The resulting distance matrix provides a comprehensive view of structural changes across quarters. To further analyse network dynamics, we apply hierarchical clustering (using the Ward linkage method) to group quarters with similar network structures. This approach highlights periods of stability and episodes of disruption in trade connectivity.

Identified clusters are then examined to interpret key periods of significant structural change, enabling a thorough assessment of how major events, such as the COVID-19 pandemic and the war in Ukraine, influenced dry bulk trade patterns. Further details on the clustering algorithm are provided in the Supplemental Materials B.

5. Results

The results are presented in two parts: (1) the static analysis of the global dry-bulk network and its coal, grain and iron ore sub-networks, and (2) the temporal analysis identifying structural breaks and community reorganisation. Throughout, we include spatial visualisations to illustrate the geographic distribution of ports and flows within each commodity-specific network, recognising, as Stopford (2008) notes, that “maritime trade analysis emphasises geographical regions over political states.”

5.1. Network properties

We begin by assessing metrics such as network size, degree distribution, assortativity, strongly connected components, and small-worldness, which together establish the essential foundation needed to interpret trade flow patterns and understand how these systems respond to external shocks.

Network size and connectivity. The full dry bulk network comprises 2748 ports and 171,631 unique trade routes, with an average in- or out-degree of 62.5 and a density of 0.023 (Table 1). Among the sub-networks, coal has the broadest port coverage (1,525 ports), grain is the most densely connected (density 0.011), and iron ore is the smallest and sparsest, served by only 902 ports and exhibiting the lowest density (0.007).

Table 1
Global network centralities of the full dry bulk network and sub-networks per commodity group. Indicators shown with full names (symbols retained in parentheses): number of ports (n); number of unique edges (e); average in- or out-degree (k); network density (ϕ); number of weakly connected components (WCCs, n_w); percentage of the giant WCC (GWCC) of the full network (p_w); diameter of the largest WCC (GWCC) (d_w); number of strongly connected components (SCCs, n_s); percentage of the giant SCC (GSCC) of the full network (p_s); diameter of the GSCC (d_s); average shortest path length (ℓ); clustering coefficient (c); and degree assortativity (a).

Network	No. of ports (n)	No. of edges (e)	Average degree (k)	Density (ϕ)	No. of WCCs (n_w)	GWCC % of full network (p_w)	Diameter (GWCC) (d_w)	No. of SCCs (n_s)	GSCC % of full network (p_s)	Diameter (GSCC) (d_s)	Avg. shortest path length (ℓ)	Clustering coefficient (c)	Degree assortativity (a)
Full Dry Bulk	2748	171,631	62.46	0.023	1	100 %	7	685	75 %	5	2.50	0.23	-0.09
Coal	1525	19,206	12.59	0.008	1	100 %	6	985	35 %	5	3.65	0.05	-0.11
Grains	1459	22,966	15.74	0.011	1	100 %	7	971	34 %	4	3.15	0.04	-0.07
Iron Ore	902	5970	6.62	0.007	1	100 %	7	738	18 %	5	4.12	0.05	-0.10

Table 2
Estimated parameters of the power-law distributions across different sub-networks. Estimated power-law exponents (γ) for different sub-networks, including: γ_all (total degree, combining in-degree and out-degree), $\gamma\_indegree$ (inbound connections), and $\gamma\_outdegree$ (outbound connections). Each row corresponds to a specific commodity sub-network as well as the full dry bulk network. We find heavy-tailed degree distributions with strong exporter-side concentration (out-degree exponent ≈ 0.7) and moderate importer-side skew (in-degree > 1); hence, not scale-free but highly concentrated.

	γ_all	γ_indegree	γ_outdegree
Dry Bulk	0.704	0.834	0.811
Coal	1.075	1.331	0.749
Grain	1.010	1.207	0.710
Iron Ore	1.069	1.328	0.761

Degree distribution. We next examine degree distribution to characterise the heterogeneity of port connectivity and to identify potential hub structures within the network. In Fig. 1, we observe heavy-tailed degree distribution in the full dry bulk network and its commodity sub-networks, consistent with power-law behaviour. The estimated exponents for total degree are 0.7 for the aggregate network and around 1.0 in the commodity sub-networks (shown in Table 2). Notably, for all sub-networks, out-degree exponents ($\gamma_{outdegree}$) are much lower (around 0.7) than in-degree exponents (equal or above 1.2). This means that export connectivity is highly concentrated among a few ports, while import connectivity, though skewed, is comparatively more dispersed.

All estimated exponents lie outside the canonical 2-3 interval for strict scale-free networks (Barabási and Albert, 1999). Thus, while the network exhibits strong heterogeneity, it cannot be considered scale-free in the classic sense. Instead, the heavy-tailed distribution points to the dominance of a small number of export hubs, whose prominence is driven by commodity-specific resource geography. As a result, network resilience depends disproportionately on the operational continuity of these key exporters. Disruption at these gateways could cause cascading effects across global dry bulk flows, particularly for commodities with limited alternative sources. Future extensions could explore multilayer or targeted-attack simulations to quantify the propagation of cascading failures and to evaluate how the removal of large, diversified ports would impact overall network resilience.

To better understand the implications of this vulnerability, it is important to clarify how hub-like structures in dry bulk differ from those observed in container and oil shipping. In liner shipping and airline networks, central hubs redistribute flows from many peripheral nodes (Newman, 2010; Ducruet, 2013, 2020). In oil shipping, hub-and-spoke patterns also emerge, but primarily due to geographic and infrastructural constraints: large crude carriers discharge at a limited number of hubs, which then redistribute via smaller vessels (Peng et al., 2019). In contrast, in dry bulk, hubs such as Port Hedland and Richards Bay serve as specialised gateways directly tied to resource locations, not as transshipment centres (Ducruet, 2020, 2013). This pattern arises from the geographic concentration of resource production and demand, rather than from network design. As a result, risk management and investment strategies should prioritise the resilience and capacity of these key export and import ports, as disruptions at these gateways can significantly impact global trade flows. Further research should also examine the mechanisms shaping hub-like structures in dry-bulk networks and how these may evolve under changing market and technological conditions.

Assortativity. Building on the evidence of hub dominance from the degree distribution, we next examine degree assortativity to evaluate how these hubs are connected within the network. Here, degree assortativity measures the tendency for ports to connect with others of similar or dissimilar connectivity. As shown in Table 1, assortativity values, a, are mildly negative or near zero across all networks, indicating a weak core-periphery (disassortative) structure and a tendency for high-degree nodes to connect to low-degree ones. Correlation analysis (Table 11, Supplementary Material A) further shows that major exporters and importers are typically distinct from one another. Positive correlations occur among same-direction centralities, while the lack of significant correlation between in-degree and out-degree highlights the asymmetric roles of most ports. Negative correlations between in-strength and out-strength, especially in grain and iron ore, reinforce this specialisation.

Overall, the patterns observed in degree distribution and assortativity demonstrate that trade imbalances are structurally embedded within the network. First, major export gateways are not necessarily the same as those for import. Second, highly connected nodes tend to link with smaller, peripheral ports. Third, exports are concentrated through a few high-volume gateways, while imports are distributed across a broader range of destinations. These patterns are further illustrated in Table 13 in Supplementary Material A, which lists the world's largest dry bulk ports according to various centrality metrics across different commodity groups. This structural configuration increases the strategic importance of key export gateways for supply chain resilience and risk management.

Spatial patterns and trade imbalances. The trade imbalances revealed by degree distribution and assortativity can be directly observed in the geographic layout of global dry bulk shipping activity. To visualise these static structural asymmetries, we map the distribution of ports and trade flows for each commodity-specific network. The complete dry bulk map (Fig. 2a) highlights the global reach of maritime trade, with most coastal countries engaged in either import or export.

Commodity-specific maps (Fig. 2b-d) reveal the underlying trade asymmetries. Exporting activity is highly concentrated: coal exports are dominated by Australia, Indonesia, Russia, South Africa, and North America; grain exports by Ukraine, Brazil, Argentina, North America, and Australia; and iron ore by a small group of resource-rich countries, notably Australia, Brazil, Canada and South Africa, with China as the principal importer. Imports, by contrast, are more widely distributed, particularly for grain, which is received across Africa, the Middle East, and Asia.

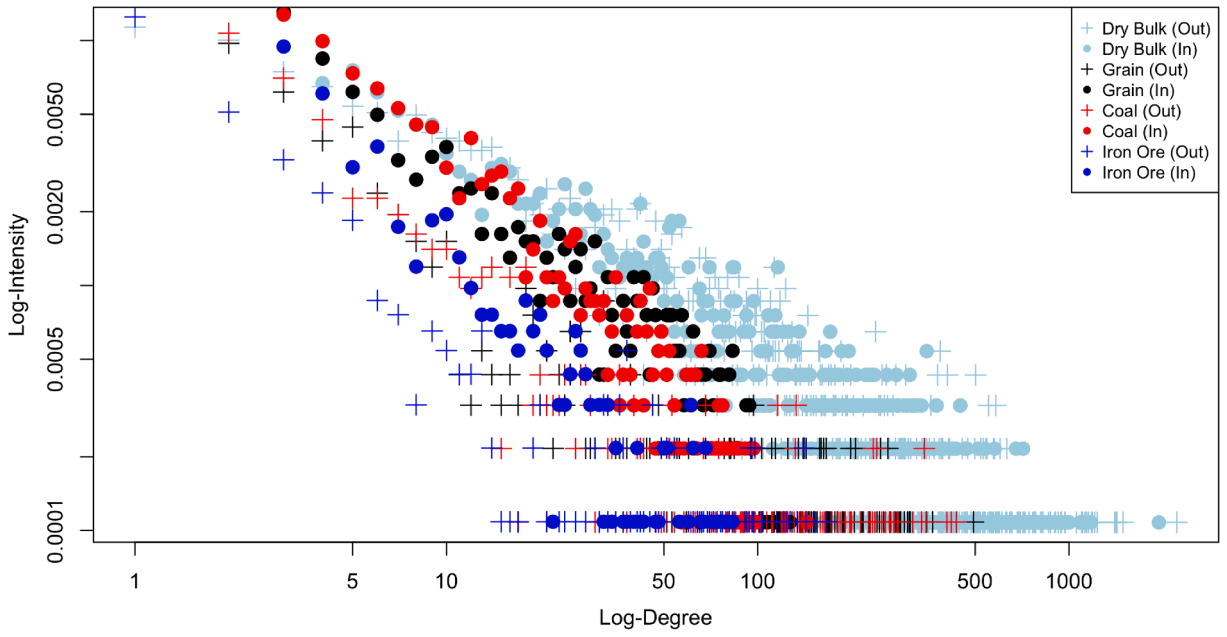

Fig. 1. Log-logdegree distributions for all sub-networks. The x-axis shows log(degree), and the y-axis shows log(frequency) of nodes with that degree. A linear trend in log–log plot indicates a power-law relationship of the form $f(k) = C\,k^{-\gamma}$, , which is consistent with the regression $\log\big(f(k)\big) = \log(C) - \gamma\,\log(k)$. The slope in these log–log plots is $-\gamma$. The plus (+) marker in the plot represents the log of out-degrees, whereas the round (∘) marker represents the log of in-degrees. A colour scheme is used to distinguish different sub-networks: light blue denotes the full dry bulk network, black represents grain, red indicates coal and dark blue signifies the iron ore sub-network. (For interpretation of the references to colour in this figure legend, the reader is referred to the web version of this article.)

The maps reinforce our earlier findings that major export nodes are few and highly central, while importing nodes are geographically dispersed. For example, within Australia, coal flows are concentrated on the east coast, iron ore on the west, and grain primarily through south Australia, corresponding directly to where major mining operations and grain-producing regions are located, and where the largest export ports have been developed to handle these specific commodities.

These spatial patterns confirm that the observed network structure, characterised by heavy-tailed degree distributions and core-periphery connectivity, emerges from highly asymmetric global trade flows. While the degree distribution and assortativity reveal some common structural features across the commodity sub-networks, the maps highlight that the geographical distribution of trade activity differs markedly by commodity. For industry stakeholders, recognising both these structural and spatial imbalances is crucial for understanding supply chain vulnerability and planning efficient routing strategies.

Spatial maps reveal overall trade imbalances but cannot fully capture the network's core-periphery structure or clustering patterns. To address this limitation, we apply component analysis to evaluate the extent of reciprocal connectivity that underpins trade resilience. We then use small-world metrics to assess the efficiency of these connections.

Component analysis. To clarify connectivity beyond aggregate statistics, we analyse the component structure of the dry bulk network and its commodity specific sub-networks (Table 1), which is a crucial factor in understanding directed network connectivity (Kiss et al., 2006). In all cases, the network forms a single weakly connected component (WCC), meaning every port is accessible when ignoring directionality. The presence of the WCC indicates complete reachability and reduced logistical barriers for international trade.

In contrast, the giant strongly connected component (GSCC), which captures ports linked by bi-directional, reciprocal flows, is much smaller: it includes 35 % of coal ports, 34 % of grain, 18 % of iron ore, and 75 % in the full dry bulk network. Ports in the GSCC typically support both import and export activity, enabling flexible, efficient routing and facilitating multi-directional exchanges of commodities. Most peripheral ports, however, act exclusively as either importers or exporters. This structural asymmetry means that these ports primarily serve a single function, either receiving shipments or sending out exports, which reinforces the global pattern whereby trade flows are dominated by a small number of gateway hubs, while the majority of ports are limited to one-way trade.

The notably smaller GSCC in iron ore reflects the extreme concentration and one-way nature of global iron ore trade. Most iron ore ports serve exclusively as exporters or importers, with few reciprocal flows between ports, in contrast to the more diversified, multi-directional exchanges seen in coal and grain. This highlights the distinctive structure of iron ore shipping, dominated by a handful of major supply and demand nodes.

When all cargo types are included, the GSCC for the full dry bulk network becomes more condensed, with higher average degrees, a larger GSCC, and shorter path lengths. This configuration promotes higher vessel utilisation by enabling charterers to move multiple commodities efficiently across the network. As visualised in Fig. 2a, overlapping node colours indicate a substantial number of ports

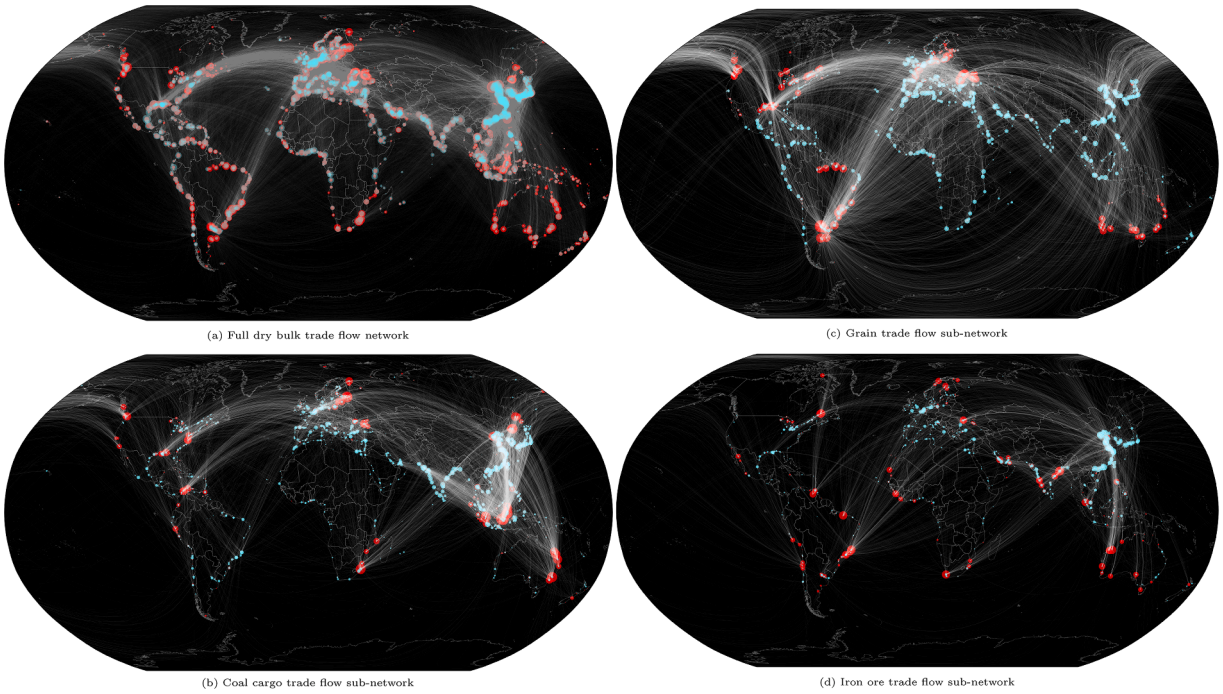

Fig. 2. Global dry bulk trade flow networks. The maps illustrate the trade flow networks for (a) the full dry bulk network, and its sub-networks: (b) coal, (c) grain, and (d) iron ore. The size of each node reflects the highest of its normalised in-degree or out-degree centralities. The nodes in red are discharge ports reflecting the out-degrees and nodes in blue are load ports reflecting in-degrees. When ports have both load and discharge activities, the two colours overlap, with the highest centrality dominating. For Map (a), we reduce line width and opacity to improve comprehension. (For interpretation of the references to colour in this figure legend, the reader is referred to the web version of this article.)

with both in- and out-degree, reflecting widespread bilateral trade flows, a contrast to the more unidirectional structures seen in the coal, grain, and iron ore sub-networks.

Network metrics reinforce this distinction: the GSCC consistently has a shorter diameter, indicating more efficient internal connectivity within the core. Practically, the size and structure of the GSCC are relevant because ports within it facilitate reciprocal trade and help minimise empty return (ballast) legs. Larger GSCCs may therefore be associated with greater potential for efficient trade, while ports outside the GSCC, relying more on single-directional flows, could be more vulnerable to disruption and operational inefficiencies, such as increased ballast activity or under-utilised vessel capacity. As noted by Brancaccio et al. (2020), while ballast legs often raise costs, assessing GSCC structures more clearly distinguishes effective bi-lateral trades and highlights network segments that may be prone to such inefficiencies. Nevertheless, establishing a direct empirical link between network topology and shipping costs requires further research.

Small-world property. Having identified a mutually accessible core through GSCC analysis, we next assess how rapidly trade and information can travel across the network by testing for small-world properties. We compare each observed network with simulated random and lattice models using the σ and ω metrics (see Methods and Table 3). The full dry bulk network demonstrates small-world features: average path length (2.50) is close to that of a random network (2.36), clustering coefficient ($C = 0.23$) is slightly higher than random ($C_{rand} = 0.22$), and both $\sigma \approx 1$ and ω are near zero. This suggests that, at the aggregate level, the network is efficiently navigable and well-integrated.

However, commodity sub-networks for coal, grain, and iron ore show more random-like structure, with lower clustering (C = 0.04-0.05) and σ and ω values only weakly indicative of small-world tendencies. This likely reflects the dominance of unidirectional flows and the sparse connectivity highlighted in our component analysis.

To clarify whether this pattern was driven by network core-periphery structure, we simulated small-world metrics for the GSCCs of each sub-network. The results are shown in Table 4. These cores display higher density and clustering (c = 0.36-0.50) and short path lengths, consistent with genuine small-world organisation. This contrast indicates that small-world characteristics are found only among those ports with dense, reciprocal trading relationships (i.e., within the GSCCs), and not across all ports in the commodity sub-networks.

The full network's clustering coefficient (0.23) is lower than in previous studies that include ballast legs (e.g., 0.43 in Kaluza et al., 2010), reflecting our focus on laden flows and reduced clique formation. As shown in Fig. 8, this highlights the impact of data definitions on network metrics. However, despite these differences, our results support the same conclusion as Kaluza et al. (2010) that the full dry bulk shipping network displays small-world characteristics.

Table 3
Network statistics of dry bulk sub-networks L denotes the observed network average path length, L_{rand} is the average path length of the rewired random graph, C is the clustering coefficient of the observed network, C_{rand} and C_{latt} represent the clustering coefficient of the rewired random graph and simulated lattice network respectively, ω and σ are the small-world measures defined by Telesford et al. (2011), Humphries and Gurney (2008).

	Network	L	L_rand	C*	C_rand	C_latt	ω	σ
1	Dry bulk	2.504	2.355	0.231	0.223	0.744	0.631	0.971
2	Grain	3.146	3.298	0.040	0.146	0.724	0.993	0.287
3	Coal	3.654	3.241	0.049	0.153	0.717	0.819	0.282
4	Iron Ore	4.120	3.581	0.049	0.150	0.682	0.797	0.285

Table 4
GSCC network statistics of real dry bulk sub-networks and simulated networks. The centrality measures of each network include: network density ϕ; number of unique edges e; number of ports n; the number of strongly-connected components (SCCs) n_s; degree assortativity a; the average shortest path length l, and clustering coefficient c.

	Dry bulk		Grain		Coal		Iron Ore	
GSCC	obs	sim.	obs	sim.	obs	sim.	obs	sim.
ϕ	0.04	0.04	0.05	0.05	0.04	0.04	0.06	0.06
e	164,110	164,110	10,985	10,985	10,968	10,968	1712	1712
n	2062	2062	489	489	541	541	164	164
$\mathbf{n_s}$	1	1	1	1	1	1	1	1
a	−0.09	−0.19	−0.07	−0.31	−0.11	−0.27	−0.16	−0.21
l	2.50	2.36	3.15	3.32	3.65	3.33	4.12	4.54
c	0.50	0.36	0.36	0.31	0.47	0.32	0.50	0.32

Furthermore, these findings indicate that the small-world properties of the GSCC facilitate efficient, multi-directional trade among ports that both import and export, supporting the circulation of raw materials, processed, and intermediate commodities within this set of reciprocally linked ports. For traders and shippers whose strategies depend on flexibility across multiple cargo types and destinations, participating in the GSCC provides access to more interconnected markets and the option to re-route vessels dynamically. In contrast, for operators focused on single-direction trade, such as iron ore exporters shipping to major importers like China, where processing is concentrated at the destination, the most operationally relevant connections are the direct, reliable export routes, even if these fall outside the GSCC.

For fleet owners and operators managing a variety of dry bulk commodities, maintaining access to the larger GSCC of the combined network enables optimised vessel deployment, higher utilisation rates, and more efficient switching between cargoes. In contrast, operating only within individual commodity sub-networks may limit routing flexibility and expose operators to greater vulnerability from trade disruptions. In addition, for supply chain management, it is essential to align operational strategies with the network structure for either reciprocal connectivity or direct commodity-specific trade routes.

5.2. Temporal analysis of networks

Building on the static analysis, this section examines how the global dry-bulk network and its main commodity sub-networks responded to major disruptions. Quarterly network reconstructions reveal the timing of structural breaks and the reorganisation of trade communities during events such as COVID-19 and the war in Ukraine.

5.2.1. Network structural change

To identify the timing of these breaks, we construct distance matrices measuring dissimilarity between quarterly network structures for coal, grain, iron ore, and the overall dry-bulk system. Fig. 10 in Supplementary Material A presents the resulting heatmaps, where darker shades denote greater structural change.

A clear divergence emerges among the commodities. The coal network (Fig. 10b) shows a pronounced structural shift in 2020, with a rapid transition to higher dissimilarity values, corresponding to the onset of the COVID-19 pandemic. Grain (Fig. 10c) is the most volatile, with persistent darker colours reflecting frequent structural changes and a particularly sharp break in early 2021, which coincides with the escalation of geopolitical tensions and the run-up to the war in Ukraine. In contrast, iron ore (Fig. 10d) displays mostly lighter, more stable patterns, with only one significant break, which occurs in 2019 (pre-pandemic), suggesting greater resilience in the face of subsequent global shocks.

The distance matrix for the full dry bulk network aggregates these patterns, showing a key structural shift in Q1 2020. Hierarchical clustering of the distance matrices (Fig. 12, Supplementary Material) reveals that, for coal and the full network, the most significant breaks align with the initial pandemic impact (Q1 2020), while for iron ore, the structural change precedes the pandemic (Q2 2019), and for grain, the break comes in Q1 2021, just before the war in Ukraine. This commodity-specific timing underlines that external shocks affected each market differently, with some responses lagging or preceding headline events.

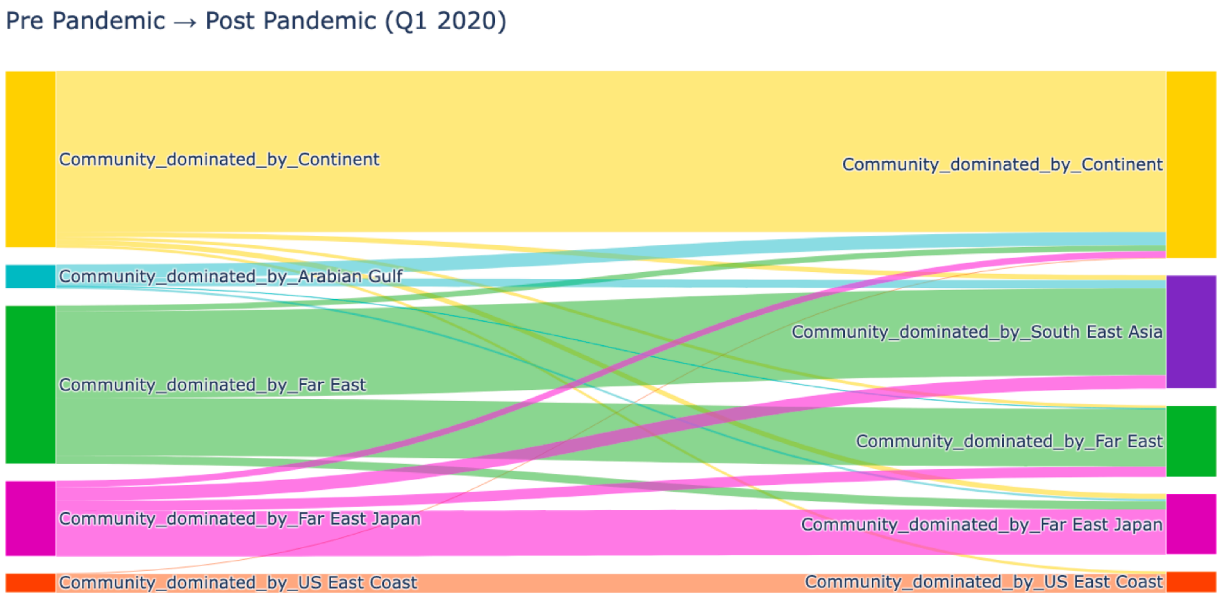

Fig. 3. Transitions in Coal Trading Communities Before and After the Pandemic: Each node (represented as rectangular blocks on either side of the diagram) corresponds to a community, with its height proportional to the community size (measured by the number of ports). Nodes are colour-coded to reflect their dominant geographical region, which is determined by counting the number of ports from each region within the community and selecting the region with the highest representation. The colour scheme matches the world maps shown below. Links between nodes represent the transitions of ports from one community to another, with the width of each link indicating the number of ports transitioning. The network prior to Q1 2020 consisted of six communities, while the post-Q1 2020 network comprises five communities. Significant changes in community structure include: (1) Communities dominated by Continent, Japan, and US East Coast remain largely unchanged. (2) Smaller communities, such as those dominated by Arabian Gulf ports and Far East Russian ports, merged with larger groups after Q1 2020. (3) The largest pre-Q1 2020 community, dominated by Far East ports, splits into two distinct communities: one dominated by China and another by Southeast Asia.

Further clustering uncovers additional transitions: for coal, a third structural cluster appears after 2022, coinciding with China's bans on Australian exports (Reuters, 2024) and increased reliance on Russian coal (Drewry, 2024) (see also Wang and Ducruet, 2014 for analysis of China's coal corridor concentration). For iron ore, a new phase emerges post-2021, coinciding with the war in Ukraine and the re-routing of major export flows. These observations demonstrate how both policy shifts and geopolitical events reshape the network structure on a quarterly basis.

A unique feature is observed in the grain network, where the distance matrix shows a periodic pattern of change, alternating strips of colour along the diagonal, which reflects the seasonality and cyclicality of global agricultural production. This pattern is not seen in coal or iron ore, highlighting the importance of accounting for inherent market cycles in shipping planning and risk assessment. We note that a detailed examination of agricultural seasonality is beyond the scope of this paper, but our results suggest it is an important avenue for future research.

Overall, this temporal analysis demonstrates that the dry bulk shipping network structure is highly sensitive to external shocks, but the timing and scale of these responses are sharply commodity-specific. For shipping and trade stakeholders, understanding when and how these breaks occur is vital for anticipating volatility, reallocating resources, and ensuring supply chain resilience in the face of both short-term disruptions and longer-term structural change.

5.2.2. Spatial distribution and evolution of community

The spatial evolution of network communities reveals how connections between major exporters and importers reorganise across periods of disruption, and reshape trade geography. Consistent with previous research (Kaluza et al., 2010; Pan et al., 2019), our results confirm that ports within the same community tend to be densely interconnected, while links between communities are sparse and often serve as critical bottlenecks. Understanding how these groupings change in response to shocks is essential for shipping companies and port authorities seeking to manage risk and optimise strategy.

Static analysis of the dry bulk network shows that community patterns largely reflect the underlying supply and demand for each commodity market. However, these patterns can shift rapidly in response to geopolitical events and market disruptions, highlighting the importance of dynamic community analysis. Here, we focus on the coal and grain networks, where such changes are especially pronounced, applying quarterly community detection with the Louvain algorithm. The resulting shifts in community structure are visualised through Sankey diagrams, which show the merging and splitting of communities over time, and world maps that geographically situate these transitions.

Coal sub-network. In the coal sub-network, where a structural break is identified in Q1 2020, we compare the detected communities before and after the break. As shown in Figs. 3 and 4, the network consisted of six communities before Q1 2020, and five afterward.

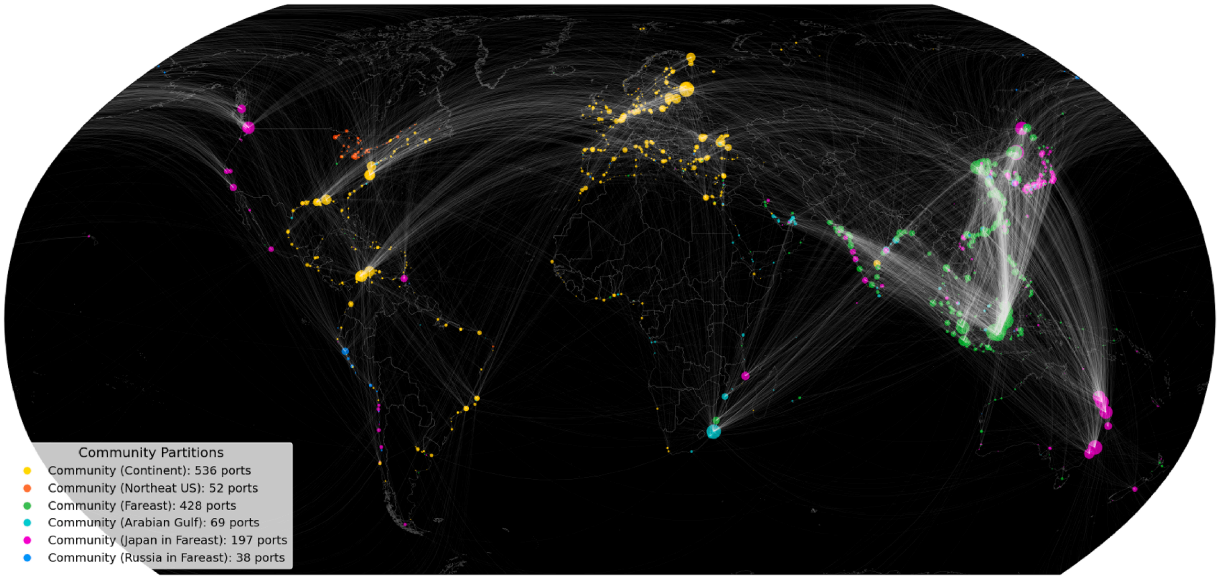

(a) Before Q1 2020

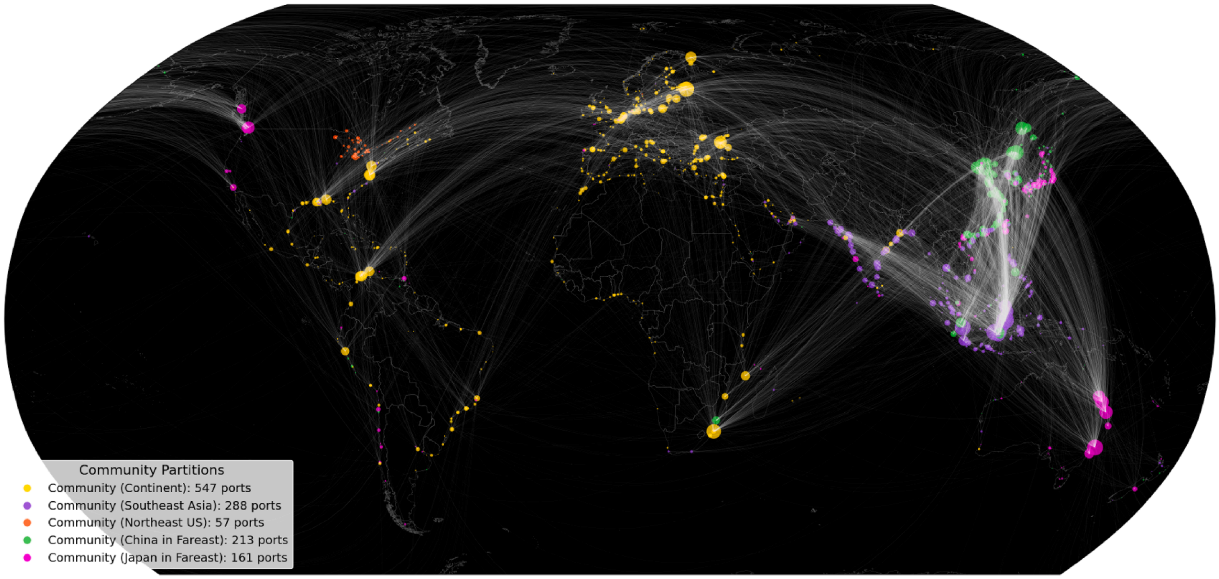

(b) Q1 2020 and After

Fig. 4. Coal handling ports and shipping routes before and after Q1 2020. Ports are grouped into communities, with distinct colours representing the dominant geographical region in each community. Dominance is determined by the region with the highest number of ports within the community. Changes in community structure are visualised through these region-specific colours, comparing the network before and after the COVID-19 pandemic (Q1 2020). The size of each node reflects the highest of its normalised in-degree or out-degree centrality. The primary structural change observable on the maps occurs in Asia (green), where ports previously grouped together split into two distinct communities: one dominated by China (green) and the other by Southeast Asia (purple). (For interpretation of the references to colour in this figure legend, the reader is referred to the web version of this article.)

The six communities identified prior to Q1 2020 are as follows: (1) the largest community, consisting of 536 ports, includes ports in Europe, North Africa, and Central America, spanning the Atlantic, Mediterranean, and Black Sea regions; (2) a community dominated by Far East ports, comprising 428 ports in total; (3) a community of 197 ports centered around Japan, East Coast Australia, and West Coast North America across the Pacific; (4) a smaller community with 52 ports, primarily located along the US East Coast; (5) a community of 69 ports concentrated in the Arabian Gulf; and (6) the smallest community, consisting of 38 ports from the Russian Far East region, spanning 17 geographical regions.

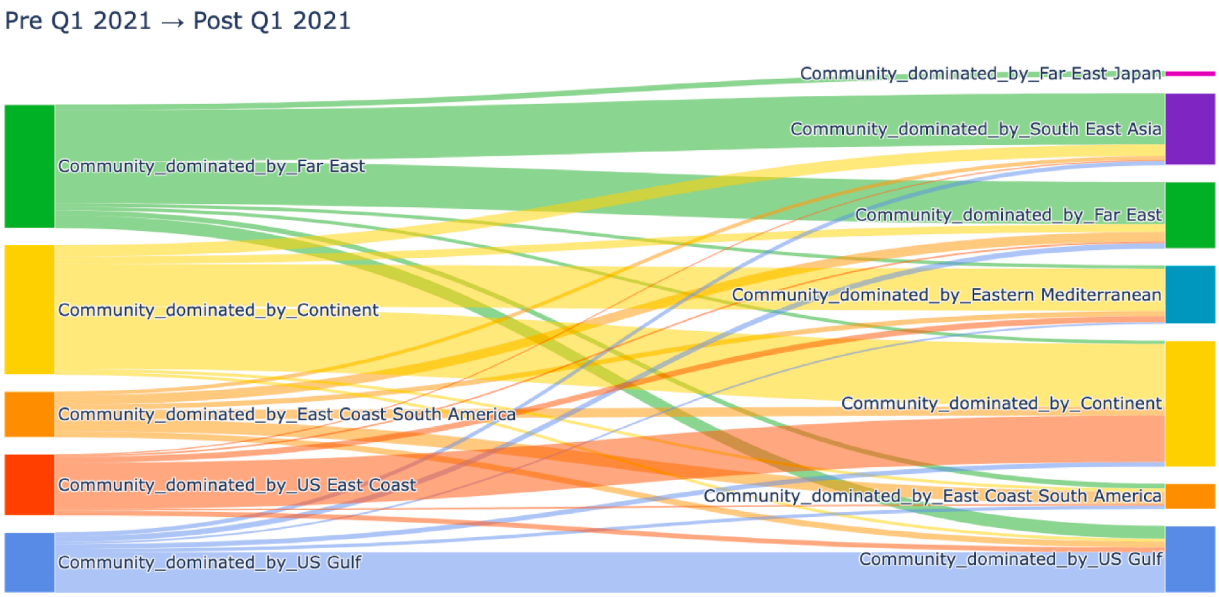

Fig. 5. Transitions in Grain Trading Communities Before and After the War in Ukraine: Each node (represented as rectangular blocks on either side of the diagram) corresponds to a community, with its height proportional to the community size (measured by the number of ports). Nodes are color-coded to reflect their dominant geographical region, determined by counting the number of ports from each region within a community and selecting the region with the highest representation. The colours used match the world maps shown below. Links between nodes represent the transitions of ports from one community to another, with each link's width indicating the number of ports undergoing that transition. The network prior to Q1 2021 consisted of five communities, while the post-Q1 2021 network comprises seven communities. Significant changes in community structure include: (1) ports in the Far East splitting into three distinct communities: one dominated by China, one by Japan, and another by Southeast Asia (2) a large community dominated by the European Continent splitting into an Eastern Mediterranean group and a remaining group still dominated by the European Continent (3) the community dominated by the US East Coast merging with the Continent-dominated community (4) most ports in the community dominated by East Coast South America transitioning to other communities, with a small proportion remaining unchanged. Finally, the community dominated by the US Gulf exhibits minimal variation.

Fig. 3 visualises the transitions in coal trading communities before and after the pandemic. Each node corresponds to a community, with its height proportional to community size and colour-coded by its dominant region. The links represent ports transitioning between communities. Prior to Q1 2020, there were six communities, while post-Q1 2020, the network comprises five communities. Significant changes include: (1) communities dominated by European Continent, Japan, and US East Coast remain largely unchanged; (2) smaller communities, such as those dominated by Arabian Gulf ports and Far East Russian ports, merged with larger groups after Q1 2020; (3) the largest pre-Q1 2020 community, dominated by Far East ports, splits into two distinct communities: one dominated by China and another by Southeast Asia.

As shown in Fig. 4, after Q1 2020, the network reconfigures into five communities. Three communities remain substantially the same as pre-Q1 2020, dominated by ports in the same regions. However, significant changes in routes across Far East Asia and the Indian Ocean after Q1 2020 lead to differences in community structure. The most notable change occurs in Asia, where a previously tightly connected group splits into two: one community is now dominated by China, while another is centred on Southeast Asian ports. Additionally, ports in the Arabian Gulf, which were previously linked to Africa, now form stronger connections with Europe and the Southeast Asia community, leaving Africa more closely aligned with Europe. Furthermore, Russian ports in Northeast Asia, which previously formed a small, distinct community with other ports, are now integrated into the same community as China, reflecting strengthened trade ties since the COVID-19 pandemic and the onset of the war in Ukraine (Drewry, 2024).

Grain sub-network. In comparison to coal, the grain shipping network exhibits a more diverse evolution in community structure.[2] As shown in Fig. 5, prior to the structural break detected in Q1 2021, the Louvain community detection algorithm identifies five communities: (1) the largest community, dominated by continental Europe, with 418 ports; (2) the second-largest community, dominated by the Far East, with 396 ports; (3) a trans-Atlantic community dominated by the U.S. East Coast, with 201 ports; (4) a community dominated by U.S. Gulf ports, with 182 ports; (5) a community dominated by East Coast South American ports, with 141 ports.

Following the structural break in Q1 2021, these five communities merge, reorganise, and ultimately form seven groups, reflecting a new grain cargo network structure. The changes can be broadly grouped into two categories: those arising in Europe from trans-

[2] Using the Louvain community detection method, we identify six communities in the pre-Q1 2021 network and eight in the post-Q1 2021 network. However, in both networks, there is a small community of fewer than five nodes, each having degree 1. In addition to the small size, since most of these nodes within the community do not appear in both networks, we exclude them from the community structure analysis in this section.

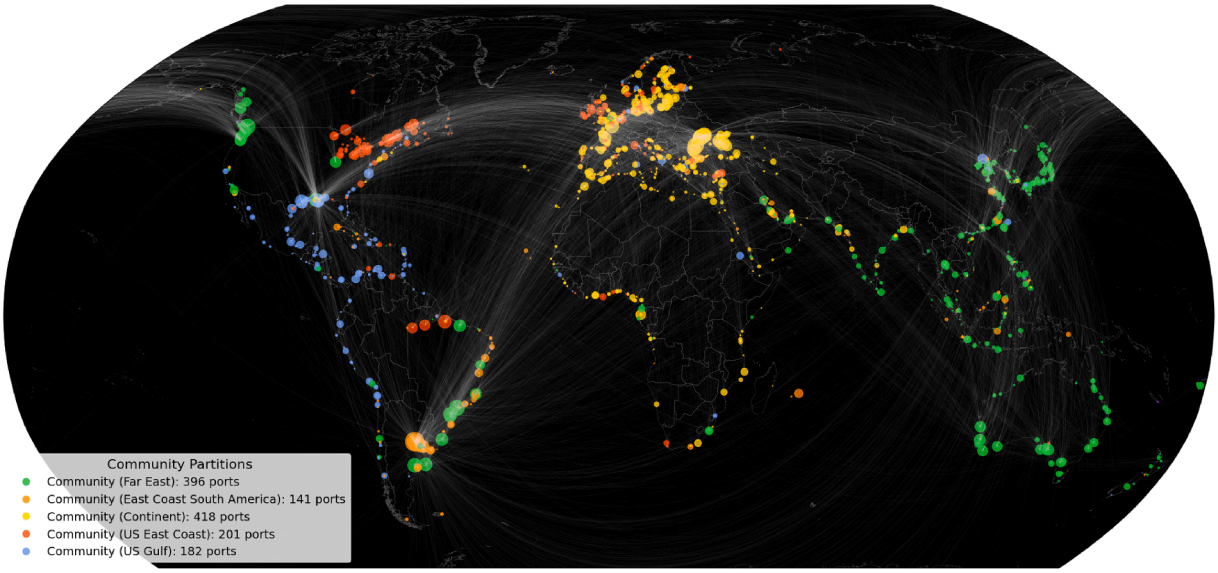

(a) Before Q1 2021

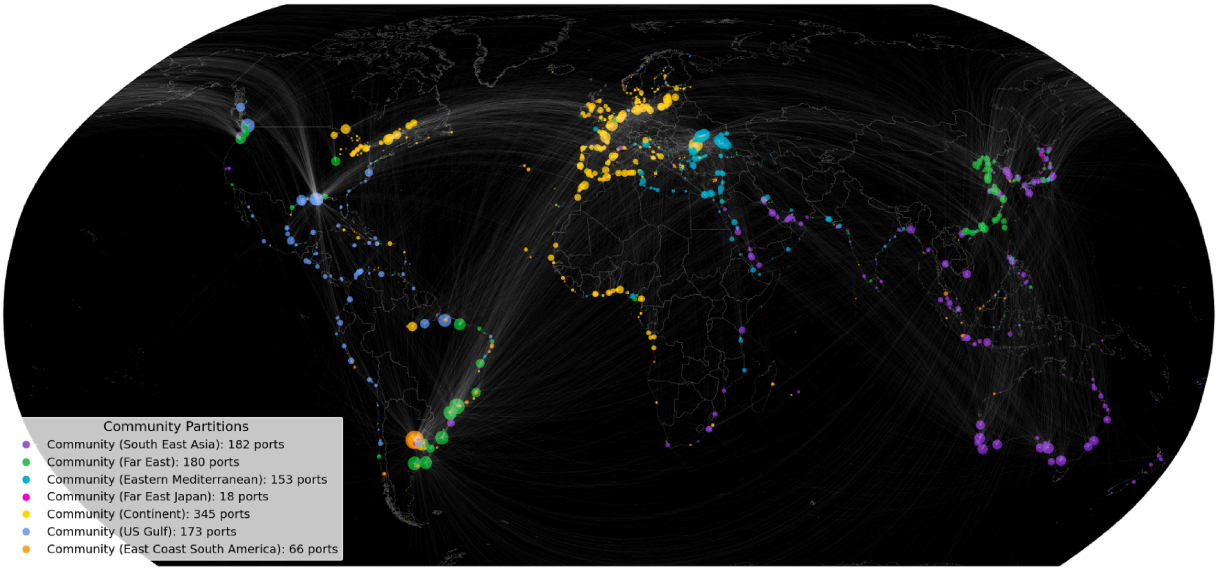

(b) Q1 2021 and After

Fig. 6. Grain handling ports and shipping routes before and after Q1 2021. Ports are grouped into communities, with distinct colours representing the dominant geographical region in each community. The community structure is visualised based on these region-specific colours before and after Q1 2021. The size of each node reflects the highest of its normalised in-degree or out-degree centrality. Significant changes in community structure include: (1) ports in the Far East splitting into three distinct communities: one dominated by China, one by Japan, and another by Southeast Asia; (2) a large community dominated by the European Continent splitting into an Eastern Mediterranean group and a remaining group dominated by Europe Continent; (3) the community dominated by the US East Coast merging with the Continent dominated community; (4) the US Gulf dominated community remains largely unchanged; (5) the East Coast South America dominated community becomes significantly smaller, as some ports transit to others. In total the number of communities increases from five to seven.

portation challenges linked to rising geopolitical tensions and the eventual outbreak of the war in Ukraine, and those arising in Asia from rising tensions between China and Australia.

For instance, the community encompassing continental Europe and North Africa is split, with ports in the Eastern Mediterranean forming a distinct group, while the former U.S. East Coast community merges into the remaining continental Europe group. Meanwhile, the smaller East Coast South American community fragments into multiple new communities, leaving only a small proportion of ports intact. The Far East community splits into three, as illustrated in Fig. 6: there are increased trade flows between Chinese ports

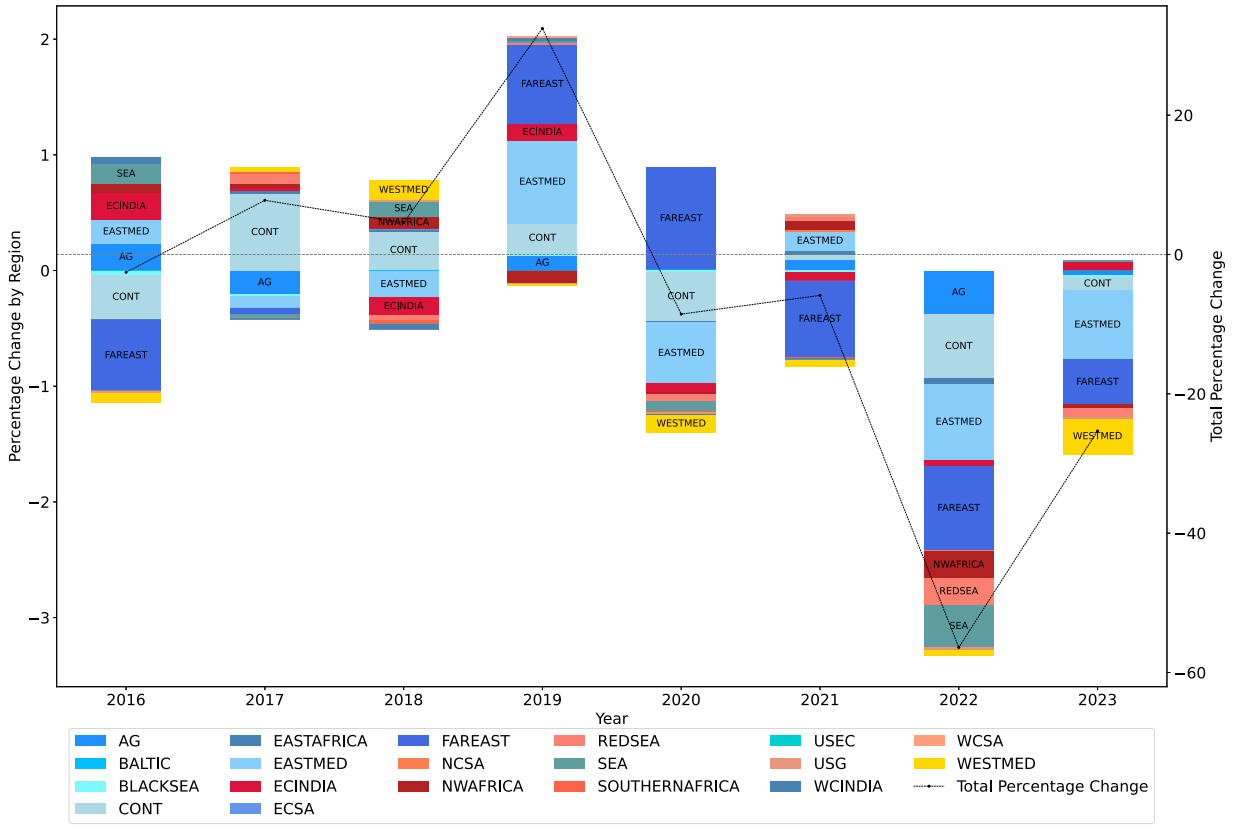

Fig. 7. Ukraine grain export volume change year on year. This figure illustrates the annual changes in grain export volumes from Ukraine from 2016 to 2023 across regions. Regions are denoted by shorthand names: AG (Arabian Gulf), EASTAFRICA (East Africa), FAREAST (Far East), REDSEA (Red Sea), USEC (East Coast US), WCSA (West Coast South America), BALTIC (Baltic), EASTMED (East Mediterranean), NCSA (North Coast South America), SEA (Southeast Asia), USG (US Gulf), WESTMED (West Mediterranean), BLACKSEA (Black Sea), ECINDIA (East Coast India), NWAFRICA (Northwest Africa), SOUTHERNAFRICA (Southern Africa), WCINDIA (West Coast India), CONT (Continent), and ECSA (East Coast South America). The volume changes are expressed as a percent change compared to the previous year. The line chart represents the total percentage change in grain exports (right y-axis), showing the aggregated impact of all regions for each year. The contribution of each region's annual change to the overall trend can be calculated by dividing the change in export volume for each year by the total change over the entire period (left y-axis). Region short names are labeled on the bars when their annual contribution exceeds 10 % in absolute value, highlighting significant regional impacts on the overall export trend.

and East Coast South America; 18 Japanese ports form a small community on their own, whereas other Asian ports form a single community led by Southeast Asia.

After Q1 2021, the network's modularity increases from 0.27 to 0.29. This is because the network becomes smaller and less dense, with fewer nodes, edges, and a reduced average degree (as shown in Table 16 in the Supplementary Materials). In a sparser network, community boundaries become more defined, as nodes cluster more distinctly.

In addition to structural changes, Fig. 7 presents year-on-year changes in Ukraine's grain export volumes. In 2021, we observe reductions in exports to the Far East and several smaller importing regions, alongside a modest recovery in shipments to the Eastern Mediterranean and North West Africa. Following the onset of the full-scale war in early 2022, Ukraine's total export volumes fell sharply, by nearly 60 % across all regions. This downward trend continued into 2023, with a further 30 % reduction in volumes. Fig. 11 in the Supplementary Material shows that global grain cargo volumes began a sustained decline starting in 2021, consistent with the timing of the observed structural break.

Although the network structure changed significantly following the identified disruptions, the countries with the highest trade volumes, measured by node strength, remained largely the same in both the grain and coal sub-networks. As shown in Table 14 in the Supplementary Materials, the composition of the top exporters and importers persisted, even as their rankings shifted slightly. In contrast, rankings based on normalised degree centrality highlight variation in the breadth of trading relationships, reflecting changes in how widely countries were connected, rather than in the absolute volume of trade.

Our findings on the structural break in the grain trade network in Q1 2021 are consistent with the analysis of Cremaschini et al. (2024). They characterise the year 2021 primarily as a pre-disruption phase, marked by gradual declines in port connectivity within Ukraine. However, their analysis focuses mainly on the impacts at the port level and the implications for Ukraine's domestic economy.

Moreover, the use of vessel movement data limits their ability to analyse commodity-specific trade patterns in detail. In contrast, our study provides new insights by identifying a structural break in Q1 2021 through quarterly network reconstructions based on micro-level trade flow data. We not only detect the timing of the transition but also trace how network topology and community composition evolved in response to emerging geopolitical tensions. By focusing on specific commodity trade networks (grain, coal, and iron ore) we are able to clearly observe how each sector responded differently to the external shock of the war in Ukraine.

6. Conclusion

This study contributes to shipping network research by integrating micro-level trade flow data with advanced network analysis to examine the organisation, resilience, and disruption of global dry bulk shipping. By analysing key commodity sub-networks (coal, grain, and iron ore), we show that these sectors differ markedly in structural properties and in their responses to external shocks.

While individual commodity networks often lack small-world features, their Giant Strongly Connected Components (GSCCs) consistently demonstrate efficient, reciprocal trade routes. These GSCCs, subsets of ports with mutual reachability, link flows of both raw and processed commodities, underpinning supply chain integration. When aggregated, the unified dry bulk network exhibits pronounced small-world and scale-free characteristics, with a relatively large GSCC indicating dense, bidirectional connectivity across regions and cargo types. Access to this extensive GSCC core enhances routing flexibility and operational efficiency, allowing fleet owners to optimise vessel deployment and repositioning within a highly connected global system.

In contrast, smaller GSCCs in individual sub-networks indicate more fragmented, uni-directional trade structures. Such asymmetry can increase ballast legs and reduce vessel utilisation, with non-GSCC components relying heavily on single-directional flows. Although this suggests higher operational costs, establishing direct links between network topology and freight economics requires further empirical analysis integrating shipping and freight data.

The results also show that dry bulk shipping networks are highly concentrated: a few hub ports handle most flows, while peripheral ports maintain limited connections. This core-periphery structure fosters efficiency but also dependency, heightening the vulnerability of smaller ports to hub disruptions. Disassortative patterns reinforce this, as smaller ports tend to connect to major hubs, deepening existing trade hierarchies and limiting diversification.

While static analysis reveals the stable geography of commodity flows, temporal analysis, using distance matrices, highlights the transformative effects of shocks. The COVID-19 pandemic triggered significant restructuring in the coal and overall dry bulk networks, whereas the grain and iron ore sectors proved more resilient. Community detection further shows how global events reshaped network topology, including closer clustering of China and Russia in the coal network. Conversely, the war in Ukraine drove dramatic realignments in the grain network, with community structures reorganised as trade routes shifted away from the Black Sea region. China's grain trade increasingly clustered with South American exporters, while Southeast Asia and Australia remained more tightly connected within the wider Asian region. The fragmentation of European and North African grain trade communities further altered connectivity, with immediate implications for trade routes and market resilience.

Beyond the impacts of global shocks, the grain sub-network exhibits a periodic pattern of structural change reflecting the seasonality of global agricultural production. This cyclical reorganisation, visible in the distance-matrix analysis, highlights the influence of recurring market cycles on trade network dynamics and the need to account for them in resilience assessments and fleet planning.

By systematically analysing static network snapshots over time, this study offers insights for commodity traders, ship owners, and logistics professionals. Recognising shifts in community structure and network topology enables adaptive routing, targeted risk mitigation, and informed strategic planning. The methodological framework developed here is generalisable, supporting context-specific analysis across other dry bulk markets and supply chains.

Future research should extend this analysis in several ways. Integrating freight rates, voyage-level cost data, and contract structures with network topology would allow a more direct assessment of how structural features influence efficiency, profitability, and market risk. Additionally, exploring multilayer network models may yield new insights into resilience, cascading failures, and the systemic effects of targeted disruptions. The seasonality observed in grain trade networks also merits further investigation, as a deeper understanding of its drivers could clarify important implications for shipping operations and supply chain risk. Methodologically, combining network analysis with causal inference approaches, such as event studies or econometric modeling, could help to more precisely quantify the effects of shocks, including policy interventions or conflicts, on trade flows and market structure. Finally, expanding both the temporal and geographic scope of analysis to encompass additional bulk segments or emerging trade corridors would offer a broader perspective on how global supply chains adapt to evolving economic and geopolitical conditions.

CRediT authorship contribution statement

Yan Li: Writing – review & editing, Writing – original draft, Visualization, Software, Methodology, Investigation, Formal analysis, Data curation, Conceptualization; **Carol Alexander:** Writing – review & editing, Visualization, Supervision, Conceptualization; **Michael Coulon:** Writing – review & editing, Supervision, Data curation; **István Zoltán Kiss:** Writing - review & editing.

Data availability

Data will be made available on request.

Declaration of interests

The authors declare that they have no known competing financial interests or personal relationships that could have appeared to influence the work reported in this paper.

Supplementary material

Supplementary material associated with this article can be found, in the online version, at 10.1016/j.tre.2025.104597

References

Bai, X., Ma, Z., Zhou, Y., 2023. Data-driven static and dynamic resilience assessment of the global liner shipping network. Transp. Res. Part E: Logist. Transp. Rev. 170, 103016.

Barabási, A.-L., Albert, R., 1999. Emergence of scaling in random networks. Science 286 (5439), 509–512.

Blondel, V.D., Guillaume, J.-L., Lambiotte, R., Lefebvre, E., 2008. Fast unfolding of communities in large networks. J. Stat. Mech: Theory Exp. 2008 (10), P10008.

Brancaccio, G., Kalouptsidi, M., Papageorgiou, T., 2020. Geography, transportation, and endogenous trade costs. Econometrica 88 (2), 657–691.

Calatayud, A., Mangan, J., Palacin, R., 2017a. Connectivity to international markets: a multi-layered network approach. J. Transp. Geogr. 61, 61–71.

Calatayud, A., Mangan, J., Palacin, R., 2017b. Vulnerability of international freight flows to shipping network disruptions: a multiplex network perspective. Transp. Res. Part E: Logist. Transp. Rev. 108, 195–208.

Cheung, K.-F., Bell, M. G.H., Pan, J.-J., Perera, S., 2020. An eigenvector centrality analysis of world container shipping network connectivity. Transp. Res. Part E: Logist. Transp. Rev. 140, 101991.

Cremaschini, F., Ducruet, C., Faure, M.-A., Polo Martin, B., 2024. Shipping Trade and Geopolitical Turmoils: The Case of the Ukrainian Maritime Network. Working Paper 2024-24. EconomiX - CNRS, University of Paris Nanterre. https://economix.fr/pdf/dt/2024/WP_EcoX_2024-24.pdf.

Drewry, 2024. China's shift towards overland metallurgical coal imports to dampen shipping demand. Accessed: 2025-06-03. https://www.drewry.co.uk/maritime-research-opinion-browser/maritime-research-opinions/chinas-shift-towards-overland-metallurgical-coal-imports-to-dampen-shipping-demand.

Ducruet, C., 2013. Network diversity and maritime flows. J. Transp. Geogr. 30, 77–88.

Ducruet, C., 2017a. Advances in shipping data analysis and modeling. Tracking and Mapping Maritime Flows in the Age of Big Data, Routledge Studies in Transport Analysis .

Ducruet, C., 2017b. Multilayer dynamics of complex spatial networks: the case of global maritime flows (1977–2008). J. Transp. Geogr. 60, 47–58.

Ducruet, C., 2020. The geography of maritime networks: a critical review. J. Transp. Geogr. 88, 102824.

Ducruet, C., Itoh, H., Berli, J., 2020. Urban gravity in the global container shipping network. J. Transp. Geogr. 85, 102729.

Ducruet, C., Lee, S.-W., Ng, A. K.Y., 2010a. Centrality and vulnerability in liner shipping networks: revisiting the northeast asian port hierarchy. Marit. Policy Manage. 37 (1), 17–36.

Ducruet, C., Notteboom, T., 2012. The worldwide maritime network of container shipping: spatial structure and regional dynamics. Global Netw. 12 (3), 395–423.

Ducruet, C., Rozenblat, C., Zaidi, F., 2010b. Ports in multi-level maritime networks: evidence from the atlantic (1996–2006). J. Transp. Geogr. 18 (4), 508–518.

Ghasemian, A., Hosseinmardi, H., Clauset, A., 2019. Evaluating overfit and underfit in models of network community structure. IEEE Trans. Knowl. Data Eng. 32 (9), 1722–1735.

Guinand, F., Pigné, Y., 2015. Time considerations for the study of complex maritime networks. In: Maritime Networks. Routledge, pp. 187–213.

Holme, P., Saramäki, J., 2012. Temporal networks. Phys. Rep. 519 (3), 97–125.

Humphries, M.D., Gurney, K., 2008. Network 'small-world-ness': a quantitative method for determining canonical network equivalence. PLoS ONE 3 (4), e0002051.

Iapadre, P.L., Tajoli, L., 2014. Emerging countries and trade regionalization. a network analysis. J. Policy Model. 36, S89–S110.

Kaluza, P., Kölzsch, A., Gastner, M.T., Blasius, B., 2010. The complex network of global cargo ship movements. J. R. Soc. Interface 7 (48), 1093–1103.

Kanrak, M., Nguyen, H.O., Du, Y., 2019. Maritime transport network analysis: a critical review of analytical methods and applications. J. Int. Logist. Trade 17 (4), 113–122.

Kiss, I.Z., Green, D.M., Kao, R.R., 2006. The network of sheep movements within great britain: network properties and their implications for infectious disease spread. J. R. Soc. Interface 3 (10), 669–677.

Kiyota, K., 2022. The COVID-19 pandemic and the world trade network. J. Asian Econ. 78, 101419.

Klimek, P., Obersteiner, M., Thurner, S., 2015. Systemic trade risk of critical resources. Sci. Adv. 1 (10), e1500522.

Laxe, F.G., Seoane, M. J.F., Montes, C.P., et al., 2012. Maritime degree, centrality and vulnerability: port hierarchies and emerging areas in containerized transport (2008–2010). J. Transp. Geogr. 24, 33–44.

Liu, C., Wang, J., Zhang, H., 2018. Spatial heterogeneity of ports in the global maritime network detected by weighted ego network analysis. Marit. Policy Manage. 45 (1), 89–104.

Newman, M.E.J., 2010. Networks: An Introduction. Oxford University Press.

Pan, J.-J., Bell, M. G.H., Cheung, K.-F., Perera, S., Yu, H., 2019. Connectivity analysis of the global shipping network by eigenvalue decomposition. Marit. Policy Manage. 46 (8), 957–966.

Peng, P., Yang, Y., Cheng, S., Lu, F., Yuan, Z., 2019. Hub-and-spoke structure: characterizing the global crude oil transport network with mass vessel trajectories. Energy 168, 966–974.

Reuters, 2024. China lifts ban on five Australian beef exporters. Accessed: 2025-06-03. https://www.reuters.com/world/asia-pacific/china-lifts-ban-five-australian-beef-exporters-2024-05-29/#: :text = China%20imposed%20the%20bans%20between,the%20origin%20of%20COVID%2D19.

Stopford, M., 2008. Maritime Economics. Taylor & Francis Ltd. 3rd edition edition.

Sugishita, K., Masuda, N., 2021. Recurrence in the evolution of air transport networks. Sci. Rep. 11 (1), 5514.

Telesford, Q.K., Joyce, K.E., Hayasaka, S., Burdette, J.H., Laurienti, P.J., 2011. The ubiquity of small-world networks. Brain Connect. 1 (5), 367–375.

Tsiotas, D., Polyzos, S., 2015. Analyzing the maritime transportation system in greece: a complex network approach. Netw. Spatial Econ. 15 (4), 981–1010.

UNCTAD, 2019. Review of maritime transport 2019. In: United Nations Conference on Trade and Development, Geneva, Switzerland. Vol. 9.

Wang, C., Ducruet, C., 2014. Transport corridors and regional balance in china: the case of coal trade and logistics. J. Transp. Geogr. 40, 3–16.

Wang, N., Wu, N., Dong, L.-l., Yan, H.-k., Wu, D., 2016. A study of the temporal robustness of the growing global container-shipping network. Sci. Rep. 6 (1), 1–10.

Wei, C., Xiao, Y., Li, L., Huang, G., Liu, J., Xue, D., 2025. After pandemic: resilience of grain trade network from a port perspective on developed and developing countries. Resour. Conserv. Recycl. 215, 108119.

Wei, N., Xie, W.-J., Zhou, W.-X., 2022. Robustness of the international oil trade network under targeted attacks to economies. Energy 251, 123939.

Williams, O., Del Genio, C.I., 2014. Degree correlations in directed scale-free networks. PLoS ONE 9 (10), e110121.

Yin, Z., Hu, J., Zhang, J., Zhou, X., Li, L., Wu, J., 2024. Temporal and spatial evolution of global major grain trade patterns. J. Integr. Agric. 23 (3), 1075–1086.

Zhang, Y.-T., Li, M.-Y., Zhou, W.-X., 2024. Impact of the russia-ukraine conflict on international staple agrifood trade networks. Foods 13 (13), 2134.